phycology

MDPI

Article

Growth Promotion of *Chlamydomonas reinhardtii* by *Cupriavidus oxalaticus* MEYA8

Xinyan Wu †, Xin Li †, Mengya Song, Jie Yu, Yuanpei Jin, Yunhao Wang * and Bo Xie *

Key Laboratory of Pesticide & Chemical Biology of Ministry of Education, Hubei International Scientific and Technological Cooperation Base of Ecology and Environment, Hubei Key Laboratory of Genetic Regulation and Integrative Biology, School of Life Sciences, Central China Normal University, Wuhan 430079, China

* Correspondence: yunhao@ccnu.edu.cn (Y.W.); xiebo@ccnu.edu.cn (B.X.)

† These authors contributed equally to this work.

Abstract

Microalgal growth-promoting bacteria (MGPBs) represent a promising strategy to enhance biomass productivity, yet the mechanistic basis of these mutualistic interactions remains poorly understood. Here, we isolated a new MGPB, *Cupriavidus oxalaticus* MEYA8, and characterized its mutualistic interaction with the model microalga *Chlamydomonas reinhardtii*. Co-cultivation at an optimal MEYA8: *Chlamydomonas* ratio greatly enhanced microalgal cell density and chlorophyll content, which reached 2.1-fold and 1.6-fold those of the control, respectively, with markedly improved photosynthetic efficiency across both photosystems. Transwell assays confirmed that this promotion is mediated by diffusible metabolites rather than direct cell contact. Metabolites and multi-omics analyses revealed that MEYA8 can produce compounds similar to indole-3-acetic acid (IAA) and is adapted to the microalgal phycosphere by preferentially utilizing organic acids and amino acid derivatives. In response, *Chlamydomonas* upregulated proteins involved in photosynthetic electron transport, energy metabolism, and nitrogen assimilation, consistent with the observed enhancement in photosynthetic performance. These findings suggest a metabolically reciprocal interaction model: MEYA8 supplies diffusible growth-promoting factors such as IAA-like compounds to enhance *Chlamydomonas* photosynthesis and growth, while *Chlamydomonas* provides organic substrates that sustain bacterial proliferation. Our work provides new insights into algal–bacterial mutualism and may provide a new microbial resource for engineering microalgal and beneficial bacterial consortia.

Keywords: microalga growth-promoting bacteria (MGPB); algal–bacterial interaction; mutualism

Check for updates

Academic Editor: Pengfei Sun

Received: 29 June 2026
Revised: 31 July 2026
Accepted: 3 August 2026
Published: 6 August 2026

Copyright: © 2026 by the authors. Licensee MDPI, Basel, Switzerland. This article is an open access article distributed under the terms and conditions of the Creative Commons Attribution (CC BY) license.

1. Introduction

Microalgae serve as fundamental primary producers in aquatic ecosystems, driving global carbon fixation and biogeochemical cycling [1]. Among them, *Chlamydomonas reinhardtii* (Chlorophyta, Chlorophyceae), a unicellular green microalga distinguished by rapid proliferation, a well-characterized genome, and photosynthetic machinery highly conserved with higher plants, has emerged as a model organism in cutting-edge research spanning photosynthesis, cellular metabolism, and synthetic biotechnology [2]. Despite its promise, the large-scale cultivation of *Chlamydomonas* remains constrained by high nutrient demands, environmental sensitivity, and low biomass yields [3].

In both natural and engineered aquatic ecosystems, microalgae often coexist with diverse bacterial communities. During growth, microalgae secrete extracellular carbo-

hydrates, organic acids, and other metabolites, constructing a unique microenvironment known as the phycosphere [4,5]. Taxonomic surveys indicate that bacterial communities within the phycosphere represent structured rather than random assemblages [6,7]. For instance, among the bacteria associated with *C. reinhardtii*, members of Pseudomonadota (particularly Alphaproteobacteria and Betaproteobacteria) and Bacteroidota are frequently enriched [8]. Some representative taxa, including Rhizobiaceae, Caulobacteraceae, Sphingomonadales, and Burkholderiales, have been frequently detected in the phycosphere bacterial community [9,10]. Within this specialized niche, microalgae and bacteria engage in intricate, dynamic interspecies interactions, where bacteria exert profound regulatory effects on microalgal growth, metabolism, and stress tolerance [8]. Microalga Growth-Promoting Bacteria (MGPB) are defined as bacterial strains that can significantly enhance microalgal growth and metabolic activity during interspecific interactions, even under adverse environmental stress conditions [11]. Accumulating evidence demonstrates that bacteria promote microalgal growth and metabolism via multiple mechanisms. This growth stimulation can be mediated by bacterial synthesis and secretion of hormones such as indole-3-acetic acid (IAA) [12–15], associations with nitrogen-fixing bacteria that may improve nitrogen availability [16–18], siderophore secretion to chelate iron [19–22], and the exchange of essential cofactors, including various vitamins crucial for microalgal physiological processes [23–27]. For instance, the strain *Emticicia* sp. EG3 has been demonstrated to enhance both the biomass and lipid content of *Euglena gracilis* [28], while *Bacillus tequilensis* significantly elevates cell density, dry weight, and the accumulation of chlorophyll and astaxanthin in *Haematococcus lacustris* [29]. Additionally, metabolites from *Bacillus*, *Mesorhizobium*, and *Phaeobacter* have been shown to boost microalgal specific growth rates by 22% to 69% [30]. Despite these advances, most studies remain correlative or focus on isolated metabolites, leaving the integrated metabolic networks and causal mechanisms of algal–bacterial mutualism largely unexplored.

All these beneficial interactions have provided insights into the development of algal–bacterial consortia to improve the biomass yield and the tolerance to stress conditions [31]. However, the bacterial diversity and specific molecular and physiological mechanisms governing growth-promoting mutualisms still remain poorly understood. In this study, we aimed to screen new MGPBs of the model green microalga, *Chlamydomonas*, and determine the underlying growth-promoting regulatory mechanism. We found that *Cupriavidus oxalaticus* MEYA8, a previously uncharacterized bacterium, can form a mutualistic interaction with *Chlamydomonas*. We further combined physiological characterization, co-culture experiments using different initial algal-to-bacterial ratios, and multi-omics analyses to systematically investigate the reciprocal metabolic adaptations of both partners. This study provides a mechanistic basis for the potential application of *Cupriavidus oxalaticus* MEYA8 in the design of synthetic microalgal–bacterial consortia and the optimization of microalgal cultivation.

2. Materials and Methods

2.1. Growth of Chlamydomonas

Chlamydomonas reinhardtii (CC1690, obtained from the Chlamydomonas Resource Center) was axenically maintained on Tris–acetate–phosphate (TAP) plate [32]. Before use, culture was assessed by microscopic examination and by spreading aliquots of the culture onto TY or R2A agar. Cultures were considered axenic when no bacteria were observed microscopically and no colonies developed on medium. The microalgal culture was incubated at 25 °C under continuous illumination at a light intensity of 120 μmol photons m^{-2} s^{-1}, with gentle agitation to maintain homogeneous growth.

2.2. Isolation and Identification of Bacteria

Water samples were collected from Nan-Lake, Wuhan, Hubei Province, China, in July 2023. The dilutions of water samples were spread on TY agar [33]. After three to six days of incubation, individual colonies were selected, and their pure cultures were identified using serial streak-plating. The purified bacteria were co-cultured with *Chlamydomonas* at different initial inoculation ratios. For taxonomic identification, 16S rRNA genes of the screened bacteria were amplified using the universal primer pair 27F (5′-AGAGTTTGATCMTGGCTCAG-3′) and 1492R (5′-TACGGYTACCTTGTTACGACTT-3′) [34] and sequenced. Amplification conditions were as follows: initial denaturation at 98 °C for 3 min and 30 cycles of denaturation at 98 °C for 10 s, annealing at 55 °C for 10 s, and extension at 72 °C for 30 s, followed by a final extension at 72 °C for 3 min. The PCR products were verified by agarose gel electrophoresis, purified using DNA Gel Extraction Kit (Simgen, Hangzhou, China), and subjected to Sanger sequencing. Sequences were blasted in EzBioCloud databases [35] to identify the closest sequences. Since the EzBioCloud results did not provide a clear species-level assignment, 16S rRNA gene sequences of type strains within the same genus were retrieved based on information from the LPSN database [36] to blast.

2.3. Estimation of Salkowski-Reactive Indole Compounds Produced by MEYA8

The production of Salkowski-reactive indole compounds was estimated using the Salkowski colorimetric method as described previously [37,38]. Briefly, the bacterium was cultured in tryptophan-supplemented medium, and the cell-free supernatant was mixed 1:1 (v/v) with Salkowski reagent. After 30 min of dark incubation, a pink color indicated IAA production.

2.4. Co-Cultivation of Chlamydomonas with Bacteria

Chlamydomonas and bacteria were separately cultured to the logarithmic growth phase. Cells of both organisms were harvested by centrifugation and washed three times with HSM [39] to remove residual nutrients and extracellular metabolites. HSM was selected for the co-cultivation experiments to establish predominantly photoautotrophic conditions and to avoid the confounding effects of exogenous carbon on bacterial growth and algal–bacterial metabolite exchange. The initial density of *Chlamydomonas* was determined using a hemocytometer. Cell density of *Cupriavidus* was determined based on the correlation between the colony forming units on plate and optical density at 600 nm. Subsequently, the alga and bacterium were co-inoculated into HSM at a defined initial inoculation ratio (1000:1 to 1:1000), and axenic mono-culture of *Chlamydomonas* was set as the control. Each group was performed in biological triplicate. All cultures were incubated at 25 °C for 7 days under continuous illumination at an intensity of 120 μmol photons m^{-2} s^{-1}.

To examine whether cell–cell contact is required, a transwell co-culture system was utilized to spatially separate the bacterium from *Chlamydomonas*. The insert was fitted with a 0.1 μm filter at the bottom, which effectively blocked the contact between microalgal and bacterial cells while permitting the free diffusion of extracellular metabolites. For co-cultivation, the bacterial suspension was inoculated into the upper insert chamber, whereas an algal suspension of *Chlamydomonas* was incubated in the corresponding lower well of the culture plate. This setup enabled the investigation of microalgal growth responses solely to diffusible metabolites secreted by the bacterium, without direct cell–cell contact.

2.5. Photosynthetic Parameter Measurement

To assess the photosynthetic characteristics of *Chlamydomonas*, three key photosynthetic parameters were determined, including chlorophyll content, the maximum photochemical

efficiency of photosystem II (PSII), and the redox induction kinetics of photosystem I (PSI) reaction center P700. Chlorophyll content was quantified following the method described by Minocha [40]. For chlorophyll fluorescence analysis, algal cells were first dark-adapted for a minimum of 20 min to ensure full relaxation of the PSII reaction centers, after which the maximum quantum yield of PSII was measured using a Water PAM chlorophyll fluorometer (Pulse-Amplitude-Modulation, Walz GmbH, Effeltrich, Germany). In parallel, P700 redox induction kinetics of *Chlamydomonas* were recorded with a JTS-10 spectrophotometer (BioLogic Science Instruments, Seyssinet-Pariset, France). Prior to detection, samples were dark-adapted for at least 5 min to eliminate light-dependent interference and ensure stable signal acquisition.

2.6. Transmission Electron Microscopy (TEM) Observation of Bacterial Morphology

The bacterium was cultured in TY liquid medium at 30 °C with shaking at 180 rpm until reaching the logarithmic growth phase. The bacterial suspension was dropped onto a copper grid and incubated for 30 s. Subsequently, the sample was negatively stained with 0.1% uranyl acetate for 1 min. After staining, the copper grid was rinsed three times with sterile water. The grid was air-dried naturally at room temperature and finally observed under a transmission electron microscope.

2.7. Metabolic Phenotype Assay Using Biolog GEN III MicroPlate™

Bacterial metabolic phenotype and substrate utilization profile were determined using a Biolog GEN III MicroPlate system (Biolog, Inc., Hayward, CA, USA), which contains 94 different phenotypic detection wells, including 71 carbon source utilization wells and 23 chemical sensitivity detection wells. Firstly, strain MEYA8 was streaked and cultured on fresh TY solid medium to obtain pure single colonies. A typical single bacterial colony was picked and suspended in the Biolog inoculating fluid, and the bacterial suspension was adjusted to the optimal turbidity required by the instrument protocol using a turbidimeter. Subsequently, the prepared bacterial suspension was evenly inoculated into each well of the GEN III MicroPlate at a volume of 100 µL per well. The inoculated microplate was incubated statically at 30 °C for 48 h. After incubation, the Biolog microbial identification system was used to read and record the absorbance value ($OD_{590\ nm}$) of each well. The positive utilization, negative utilization, and marginal utilization of different carbon sources and the tolerance response to various chemical stressors of strain MEYA8 were analyzed based on the color reaction and turbidity changes in each well.

2.8. Third-Generation Bacterial Genome Sequencing

Whole-genome sequencing of strain MEYA8 was performed by Beijing Biomarker Technologies Co., Ltd. (Beijing, China). A ligation-based Nanopore library was prepared using the Ligation Sequencing Kit 1D (SQK-LSK109; Oxford Nanopore Technologies, Oxford, UK), and the flow cell was primed using the Flow Cell Priming Kit (EXP-FLP001.PRO.6; Oxford Nanopore Technologies, Oxford, UK). Long-read sequencing was conducted on a PromethION 48 instrument using a PromethION flow cell (FLO-PRO002, R9.4.1; Oxford Nanopore Technologies, Oxford, UK). Raw sequencing signals in FAST5 format were base-called with Guppy v3.2.6, followed by removal of adapters and quality control. The filtered long reads were de novo assembled using Canu v1.5, and the assembly was further polished with Illumina NovaSeq 6000 short-read data using Pilon v1.22. Protein-coding genes were predicted using Prodigal v2.6.3, and tRNA genes were identified using tRNAscan-SE v2.0, whereas rRNA genes and other non-coding RNAs were predicted using Infernal v1.1.3 against the Rfam database. Functional annotation was performed by comparison against NCBI non-redundant protein sequence database (NR), KEGG, eggNOG, Swiss-Prot,

and TrEMBL databases, with Gene Ontology (GO) and Pfam annotations assigned using Blast2GO v2.5 and HMMER v3.0, respectively.

2.9. Proteomics Analysis

Protein expression levels were quantified using a label-free proteomics approach. After 7 days of cultivation in HSM, mono-cultures and co-cultures were harvested by centrifugation (5000× *g*, 10 min, 4 °C). Cell pellets were immediately snap-frozen in liquid nitrogen and stored at −80 °C until further processing. Total protein extraction and sample preparation were performed following the label-free quantitative proteomics protocol described by Zhao et al. [41]. Briefly, frozen cell pellets were resuspended in ice-cold lysis buffer (2% SDS, 40 mM Tris base, pH 8.5, 60 mM DTT) supplemented with 1× protease inhibitor cocktail (Roche) to prevent proteolytic degradation. Cells were disrupted by ultrasonic homogenization (135 W, 5 s on/5 s off, 10 min) on ice, followed by centrifugation at 13,000× *g* for 10 min at 4 °C to remove insoluble cell debris. The protein concentration in the supernatant was determined using a BCA protein assay kit (Beyotime Biotechnology, Shanghai, China) with bovine serum albumin (BSA) as the standard. Total protein (100 μg) extracted from each sample was subjected to subsequent experiments. Protein reduction was achieved by incubating samples with 10 mM DTT at 56 °C for 30 min, followed by alkylation with 55 mM iodoacetamide in the dark at room temperature for 30 min. Trypsin (Promega Corporation, Madison, WI, USA) was added at a 1:50 (enzyme: protein) ratio, and digestion was carried out at 37 °C for 16 h with gentle shaking. The resulting peptide samples were analyzed using an Exactive Plus Orbitrap mass spectrometer (Thermo Fisher Scientific, Bremen, Germany) coupled to an EASY-nLC 1200 system (Thermo Fisher Scientific, Rockford, IL, USA). Approximately 1 μg of peptide sample was loaded onto a C18 column with a pore size of 150 Å, a length of 15 cm, and an internal diameter of 100 μm and separated at a flow rate of 300 nL/min over 120 min. Peptides were eluted using a segmented linear gradient of mobile phase B from 10% to 80%, with mobile phase A consisting of 5% acetonitrile and 0.1% formic acid and mobile phase B consisting of 90% acetonitrile and 0.1% formic acid. The eluted peptides were ionized by nanoelectrospray ionization at a spray voltage of 2.0 kV. Mass spectrometric analysis was performed in data-dependent acquisition mode. Full MS precursor scans were acquired over a mass range of 350–2000 m/z at a resolution of 70,000. The 20 most abundant precursor ions from each full scan were selected for higher-energy collisional dissociation fragmentation. MS/MS spectra were acquired in the Orbitrap at a resolution of 17,500 using an isolation window of 1.8 m/z. The dynamic exclusion duration was set to 40 s, and the automatic gain control target was set to 5×10^4 [42].

To compare protein expression profiles between co-culture and monoculture systems, the distributed normalized spectral abundance factor (dNSAF) was calculated for each identified protein according to the algorithm in the previous literature [43,44]. Differentially expressed proteins of bacteria in co-culture versus mono-culture systems were identified through pairwise comparisons. Natural log-transformed dNSAF data were compared using Student's *t*-test in GraphPad Prism (version 8.0.1; GraphPad Software, Boston, MA, USA). Proteins with a fold change greater than or equal to 1.5 and a *p*-value below 0.05 were identified as significantly differentially expressed proteins (DEPs). Subsequently, KEGG functional enrichment analysis of these DEPs was performed using TBtools-II v2.463 [45], and their related metabolic pathways were further annotated and analyzed with reference to the KEGG pathway database.

2.10. Effects of Exogenous Phytohormones and Vitamins on Chlamydomonas

Chlamydomonas cells cultured to the logarithmic growth phase were collected by centrifugation, washed three times with HSM to remove residual culture components, and resuspended to obtain an axenic algal suspension. For the exogenous supplementation tests, IAA was added to the algal suspension at a series of concentrations, 0.1, 0.2, 0.5, 1, 3, 5, and 10 mg/L; vitamin B_1 (VB_1) was added at 0.01, 0.05, 0.1, 0.5, 1, 5, and 10 mg/L; vitamin B_7 (VB_7) was added at 0.01, 0.05, 0.1, 0.5, 1, 5, and 10 μg/L. *Chlamydomonas* cell density and chlorophyll content were determined to compare the effects of supplementations on growth.

3. Results

3.1. Growth Promotion Effect of Chlamydomonas by Bacterial Isolates

In this study, we isolated bacterial strains from a water sample collected from Nan-Lake in Wuhan. Co-culture screening with *Chlamydomonas* revealed strain-specific effects on algal growth (Figure S1a). Among the tested 27 isolates, strain MEYA8 consistently elicited the most substantial increases in chlorophyll content and was selected for further characterization.

Co-cultivation of *Chlamydomonas* with MEYA8 exhibited in a bacterial: algal inoculum ratio-dependent effect on *Chlamydomonas* growth. Across the tested ratios (1:1000 to 1000:1), the growth-promoting effect peaked at 100:1 (Figure 1a, Figure S1b). At this optimal initial inoculum ratio, strain MEYA8 significantly promoted *Chlamydomonas* growth through growth dynamic monitoring (Figure 1b). Concurrently, bacterial cell density also increased progressively throughout the co-cultivation (Figure 1c). We also found the presence of MEYA8 significantly increased the maximum quantum efficiency of PSII (Fv/Fm, about 1.2-fold) relative to the axenic control ($p < 0.001$, Figure 1d). Consistently, chlorophyll fluorescence induction kinetics revealed a significantly amplified light-induced fluorescence change $(\Delta I/I)_{705\,nm}$ in co-cultured *Chlamydomonas* (Figure 1e), reflecting stronger photochemical quenching and higher electron transport efficiency through PSI. These data indicated that growth and photosynthetic performance of *Chlamydomonas* are promoted in the co-cultures. We further conducted the co-cultivations using the transwell system to separate the direct bacterial–microalgal contacts. Diffusible metabolites significantly increased *Chlamydomonas* cell density and chlorophyll content relative to the axenic control (Figure 1f,g), implying that this promotion is cell–cell contact-independent.

3.2. Taxonomic Assignment of Strain MEYA8

Comparison of the 16S rRNA gene sequence of MEYA8 indicated that its closest match was *Cupriavidus oxalaticus* DSM 1105^T, with a sequence similarity of 99.25%. Phylogenetic analysis (Figure 2a) demonstrated that strain MEYA8 and *Cupriavidus oxalaticus* formed a separated clade, indicating a close evolutionary relationship. These phylogenetic results indicated strain MEYA8 belongs to the genus *Cupriavidus*. Whole-genome comparison further showed that MEYA8 shared an ANI value of 99.40% and a dDDH value of 78.3% with *C. oxalaticus* DSM 1105^T. Both values were above the generally accepted species-level thresholds of 95–96% for ANI and 70% for dDDH [46], supporting the identification of MEYA8 as a strain of *Cupriavidus oxalaticus* (*Cupriavidus*).

Cupriavidus MEYA8 formed translucent and moist colonies with smooth surfaces and irregular margins. TEM observation showed that MEYA8 cells were short rod-shaped to ovoid in shape, approximately 1.0–1.5 μm in length and 0.5–0.8 μm in width, with a smooth and continuous cell envelope (Figure 2b). Long, thin, peritrichous flagella were observed on the cell surface, suggesting potential motility.

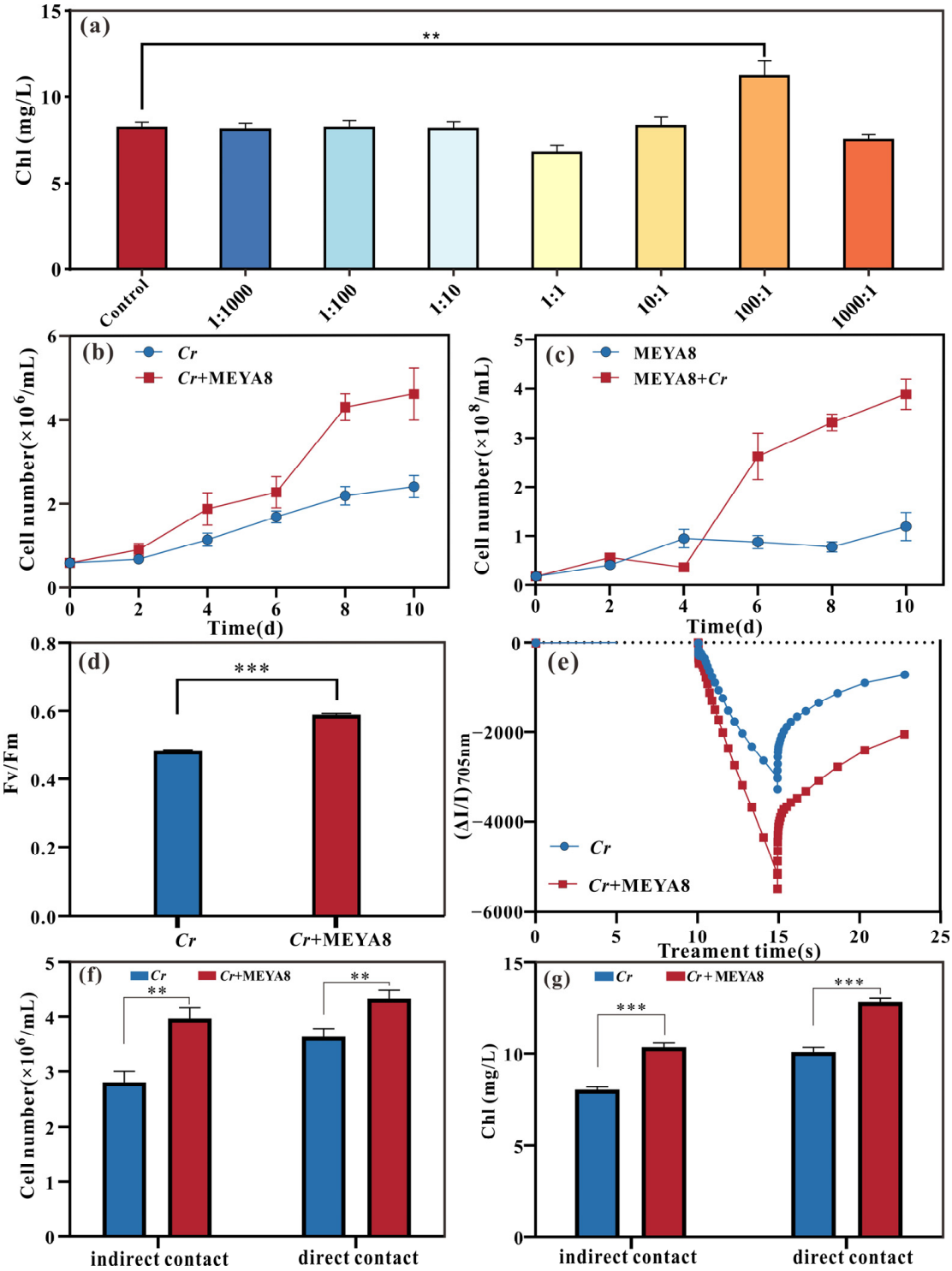

Figure 1. Growth-promoting effect of strain MEYA8 on *Chlamydomonas* and co-culture growth dynamics. (**a**) Effects of different ratios of strain MEYA8 on the chlorophyll content of *Chlamydomonas* (*Cr*). (**b**) Growth curve of *Chlamydomonas* co-cultured with strain MEYA8 in HSM at a bacterial-to-algal inoculation ratio of 100:1. (**c**) Growth curve of strain MEYA8 co-cultured with *Chlamydomonas* in HSM at a bacterial-to-algal inoculation of 100:1. (**d**) The maximum quantum efficiency (Fv/Fm) of PSII in *Chlamydomonas* under co-culture with strain MEYA8. (**e**) P700 oxidation–reduction kinetics of *Chlamydomonas* under co-culture with strain MEYA8. (**f**,**g**) Effects of direct and indirect co-culture (physically separated by transwell) on *Chlamydomonas* cell number (**f**) and chlorophyll content (**g**). (Values are means ± SD (n = 3). Statistical significance was determined by t-test. Asterisks indicate significant differences from the control: ** $p < 0.01$, and *** $p < 0.001$.)

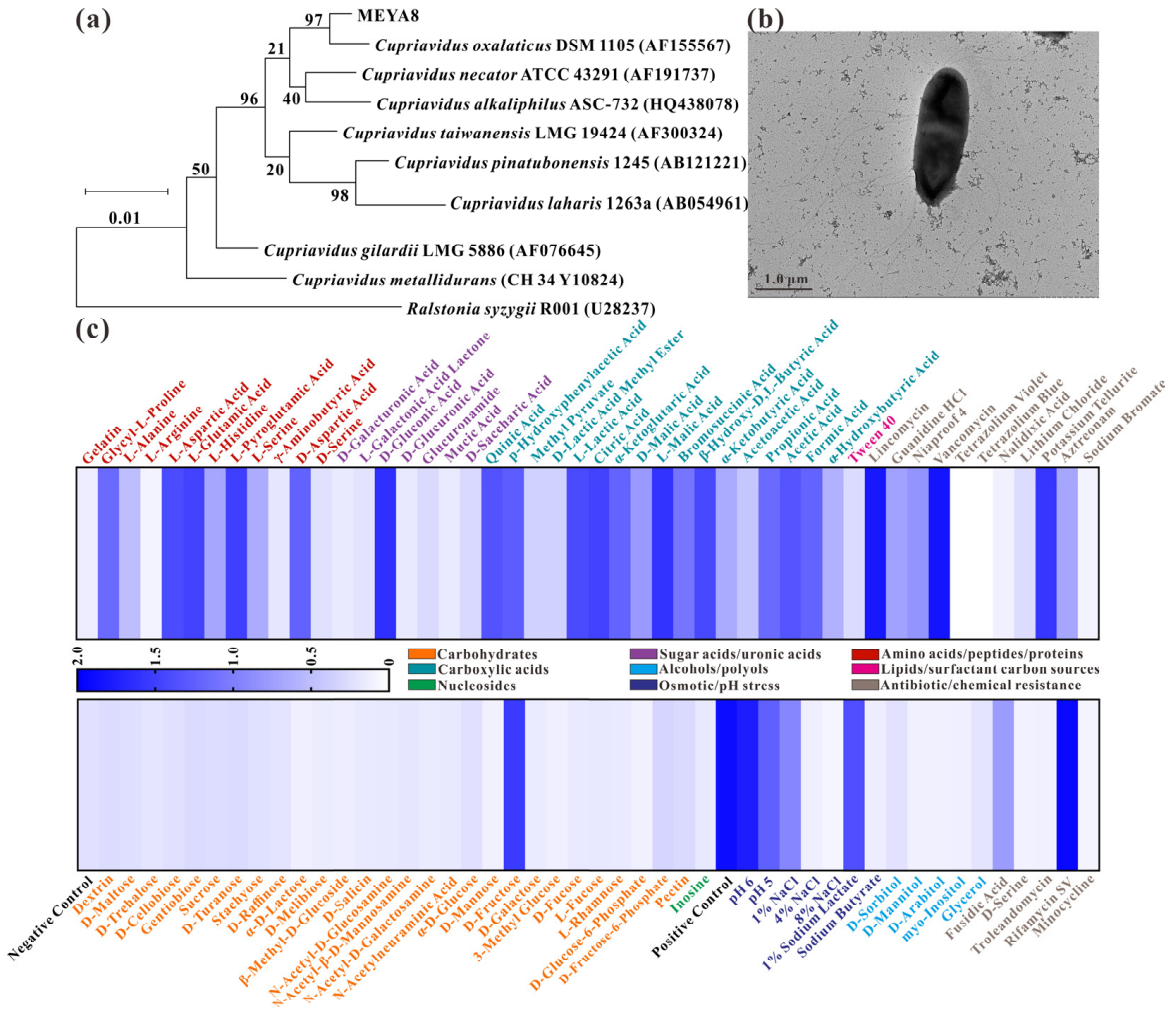

Figure 2. Taxonomic identification and physiological characterization of strain MEYA8. (**a**) Phylogenetic tree of MEYA8. Phylogenetic tree indicating the relationship of the 16S rRNA gene sequence of MEYA8 to those representative related bacterial strains. The phylogenetic tree was constructed using the neighbor-joining method. Bootstrap values (1000 replicates) are shown at the branches. The tree is drawn to scale, with branch lengths indicating evolutionary distances. *Ralstonia syzygii* R001 was used as the outgroup. The scale bar of 0.01 represents the genetic distance. GenBank accession numbers of closely related strains are shown in parentheses. (**b**) Transmission electron microscopy (TEM) image of strain MEYA8. A rod-shaped cell with flagella was shown at 10,000× magnification, with a scale bar of 1.0 μm. (**c**) Metabolic profile of strain MEYA8 obtained using the Biolog GEN III MicroPlate. The heatmap shows the utilization intensity of 94 test wells, represented by absorbance values at 590 nm (A_{590}). The color gradient from white to dark blue indicates increasing utilization intensity (0–2.0, truncated at 2.0).

Phenotypic profiling using Biolog GEN III microplates revealed that strain MEYA8 exhibited relatively weak utilization of most carbohydrates and sugar alcohols but showed stronger metabolic activity toward organic acids (e.g., L-malic acid, β-hydroxy-D,L-butyric acid, L-lactic acid, and citric acid) and selected amino acid derivatives (e.g., glycyl-L-proline, L-aspartic acid, L-glutamic acid, and L-pyroglutamic acid) (Figure 2c). In addition, the strain exhibited weaker growth at pH values below 6 and under high-salt conditions (NaCl > 1%). These results indicated that strain MEYA8 was characterized by preferential utilization of organic acids, moderate tolerance to mildly acidic conditions, and adaptability to low-salinity environments, which may facilitate its colonization of the *Chlamydomonas* phycosphere.

3.3. Genomic Characterization and Functional Validation of Growth-Promoting Traits

The MEYA8 genome assembly comprised three contigs, including two large chromosomes (chromosome 1: 3,669,605 bp and chromosome 2: 2,397,653 bp) and a putative plasmid (contig00003: 603,547 bp). This multipartite architecture is characteristic of the genus *Cupriavidus* and aligns with closely related strains such as *C. necator* JMP134, *C. metallidurans* CH34, and *Cupriavidus* sp. Agwp_2 [47–49]. Circular maps depicting genomic features (GC content, GC skew, sequencing depth, and coding gene distribution) are shown in Figure 3a. The 6.67-Mb genome exhibits a GC content of 66.56% and encodes 6019 predicted proteins.

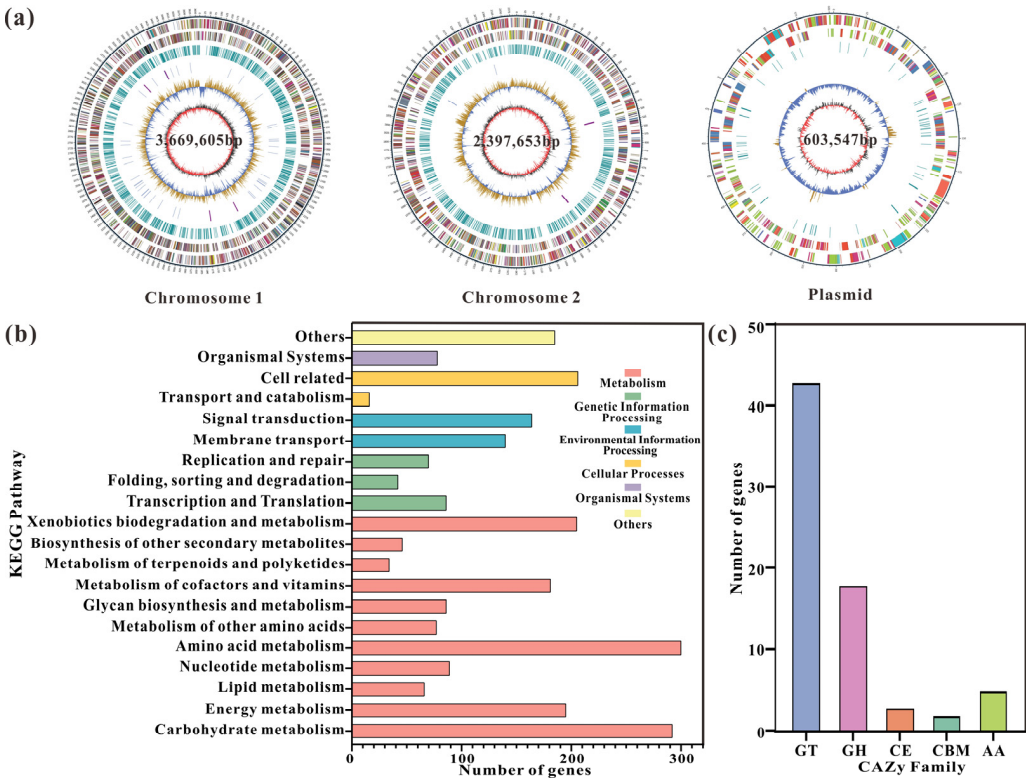

Figure 3. Genomic analysis and functional annotation of *Cupriavidus* MEYA8. (**a**) Circular maps of the chromosomes and plasmid of MEYA8. The outermost circle indicates the genome size with a scale of 5 kb per tick. The second and third circles represent genes on the positive and negative strands, respectively, with different colors corresponding to various COG functional categories. The fourth circle shows repetitive sequences. The fifth circle displays tRNA and rRNA genes, with tRNA in blue and rRNA in purple. The sixth circle represents the GC content: light yellow regions indicate higher GC content than the genome average, with higher peaks representing greater deviation; blue regions indicate lower GC content than the average. The innermost circle shows the GC-skew: dark gray represents regions with G > C, and red represents regions with C > G. (**b**) KEGG pathway classification for the MEYA8 genome. Different colors represent the KEGG level-1 functional categories, including Metabolism (red), Genetic Information Processing (green), Environmental Information Processing (blue), Cellular Processes (orange), Organismal Systems (purple), and Others (yellow). (**c**) CAZyme prediction for the MEYA8 genome. GT: Glycosyltransferase; GH: Glycoside hydrolase; CE: Carbohydrate esterase; CBM: Carbohydrate-binding module; AA: Auxiliary activity enzymes.

KEGG functional annotation assigned the predicted genes of MEYA8 to various biological pathways, with the largest proportion assigned to metabolism (Figure 3b). Specifically, amino acid metabolism (300), carbohydrate metabolism (292), xenobiotic biodegradation and metabolism (205), and energy metabolism (195) constituted the largest functional categories. Notably, a substantial number of genes were assigned to signal transduction

(164) and membrane transport (140), suggesting the potential involvement of MEYA8 in environmental sensing and nutrient exchange. In contrast, genetic information processing (198), cellular processes (222), and organismal systems (78) accounted for relatively smaller proportions of the genome. Additionally, we characterized the CAZyme repertoire of MEYA8. Genome mining identified 71 CAZyme-related genes, comprising 43 glycosyltransferases (GTs), 18 glycoside hydrolases (GHs), 5 auxiliary activity enzymes (AAs), 3 carbohydrate esterases (CEs), and 2 carbohydrate-binding modules (CBMs) (Figure 3c).

We conducted a targeted analysis of genes associated with growth-promoting traits, particularly focusing on phytohormone and vitamin biosynthesis. Genomic annotation revealed that MEYA8 harbors complete biosynthetic pathways for IAA, thiamine (VB_1) and biotin (VB_7) (Table S1). Specifically, the strain encodes a complete IAA biosynthetic pathway via the indole-3-pyruvic acid (IPyA) route (Figure S2a). This capability was experimentally confirmed by the detection of MEYA8 culture (Figure S2b). To evaluate the physiological relevance of these compounds, we tested their effects on *Chlamydomonas* growth. Exogenous IAA exerted a dose-dependent hormetic effect on the growth of *Chlamydomonas* (Figure S2c,d): low concentrations (0.1–0.5 mg/L) significantly promoted *Chlamydomonas* proliferation and chlorophyll accumulation, whereas high concentrations ($\geq$3 mg/L) inhibited its growth. In contrast, exogenous supplementation with VB_1 or VB_7 did not yield a clear growth-promoting effect under our conditions (Figure S2e–h).

3.4. Comparative Proteomic Analysis of MEYA8

Comparative proteomics analysis of *Cupriavidus* MEYA8 under co-culture and monoculture identified 897 differentially expressed proteins, with 313 upregulated and 584 downregulated (Figure 4a). KEGG enrichment analysis revealed that the upregulated proteins were predominantly associated with central carbon metabolism (32 protein assignments), amino acid biosynthesis/metabolism (39), and energy metabolism (28) (Figure 4b). Specifically, regarding carbon utilization and energy generation, the glyoxylate and dicarboxylate metabolism pathway showed the strongest enrichment, with 16 upregulated proteins (rich factor = 3.059, adjusted p value < 0.001) (Figure 4d). Proteins such as Acs (acetyl-CoA synthetase) [Fold change (FC) = 1.66, $p < 0.05$], GckA/GlyctK (glycerate kinase) (FC = 1.84, $p < 0.05$), and Gph (2-phosphoglycolate phosphatase/phosphoglycolate phosphatase) (FC = 5.57, $p < 0.01$) were significantly upregulated, suggesting enhanced uptake and conversion of algal-derived organic carbon. Concurrently, the pentose phosphate pathway appeared to be enhanced, with increased abundance of Zwf (glucose-6-phosphate dehydrogenase), Pgl (6-phosphogluconolactonase), Rpe (ribulose-phosphate 3-epimerase), and TktA/TktB (transketolase), whose FC values ranged from 1.53 to 2.55 ($p < 0.05$), indicating enhanced carbon flux and NADPH generation. Proteins related to oxidative phosphorylation were also upregulated, collectively helping to maintain high metabolic activity in the phycosphere. Proteins involved in respiratory electron transport and ATP synthesis were upregulated, including NuoA/NuoD/NuoL/NuoM (NADH-quinone oxidoreductase subunits), CoxA/CoxB and CcoN (cytochrome c oxidase subunits), CydA (cytochrome bd ubiquinol oxidase subunit I), and AtpD/AtpH/AtpE (F-type ATP synthase subunits), suggesting enhanced respiratory activity and ATP generation. Furthermore, enzymes involved in aromatic amino acid biosynthesis, including AroQ (chorismate mutase), AroC (chorismate synthase), and TyrB (aromatic-amino-acid aminotransferase), were upregulated. Crucially, TrpA (tryptophan synthase alpha chain) and TrpB (tryptophan synthase beta chain), which catalyze the final steps of tryptophan biosynthesis, a precursor of IAA, were significantly upregulated, with FC values of 2.95 and 1.52 ($p < 0.05$), respectively, suggesting metabolic reprogramming to fuel IAA production during co-cultivation.

In contrast, the down-regulated proteins were predominantly associated with genetic information processing and cellular proliferation (Figure 4c). Most notably, a broad decrease in 16 ribosomal proteins, such as RpmI (50S ribosomal protein L35), RplT (50S ribosomal protein L20), RpmB (50S ribosomal protein L28), and RpsG (30S ribosomal protein S7), with FC values ranging from 0.15 to 0.53, indicated substantially reduced translational activity at the sampling time point (Figure 4e). Similarly, six proteins involved in DNA replication and repair, including DnaB (Replicative DNA helicase), DnaX (DNA polymerase III subunit tau/gamma), and UvrA (Excinuclease ABC subunit A), were down-regulated, reflecting reduced cellular investment in proliferation. Additionally, proteins related to protein secretion, glutathione metabolism, and secondary metabolism showed decreased abundance.

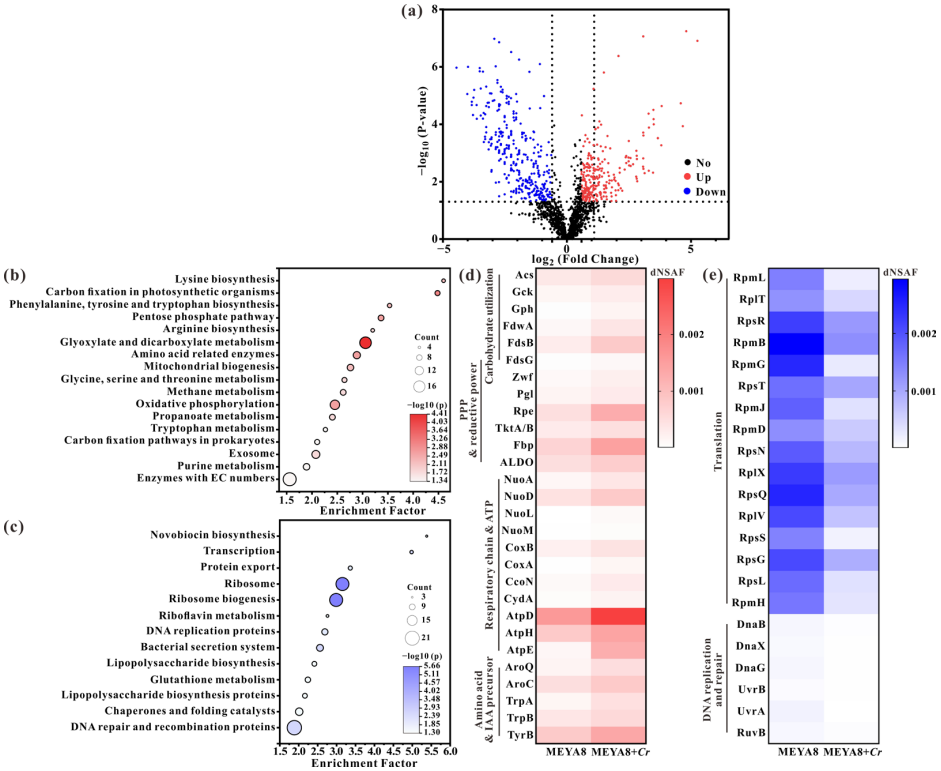

Figure 4. Proteomic pathway enrichment of differentially expressed proteins in *Cupriavidus* MEYA8 under co-culture versus monoculture conditions. (**a**) Volcano plot of differentially expressed proteins in *Cupriavidus* MEYA8 under co-culture versus monoculture conditions. The *x*-axis represents $\log_2$ fold change (co-culture/monoculture), and the *y*-axis represents $-\log_{10}$ (*p*-value). The horizontal dashed line indicates the significance threshold ($p < 0.05$), and the vertical dashed lines indicate the fold-change thresholds for upregulated and downregulated proteins, corresponding to FC > 1.5 and FC < 0.66. Red dots: significantly upregulated proteins; blue dots: significantly down-regulated proteins; black: proteins with no significant difference. (**b**) KEGG pathway enrichment bubble plot of up-regulated proteins in *Cupriavidus* MEYA8 under co-culture versus mono-culture conditions. (**c**) KEGG pathway enrichment bubble plot of downregulated proteins in *Cupriavidus* MEYA8 under co-culture versus monoculture conditions. (**d**) Heatmap of key proteins in upregulated pathways under co-culture versus monoculture conditions. (**e**) Heatmap of key proteins in down-regulated pathways under co-culture versus monoculture conditions.

3.5. Comparative Proteomic Analysis of Chlamydomonas

Comparative proteomic analysis of *Chlamydomonas* under co-culture with MEYA8 and monoculture conditions identified 853 differentially expressed proteins, including 244 upregulated and 609 down-regulated proteins in the co-culture group (Figure 5a). Regarding the upregulated proteins, KEGG enrichment analysis and heatmap visualization

(Figure 5b,d) revealed three major functional modules. First, photosynthetic machinery appeared to be enhanced, with up-regulation of photosynthesis-related pathways (photosynthesis and photosynthesis antenna proteins) and increased abundance of key components of photosynthetic electron transport complexes [e.g., PSAE (photosystem I subunit E), PETC (cytochrome b6f complex Rieske iron-sulfur subunit), and LHCBM4 (light-harvesting chlorophyll a/b-binding protein), with FC values of 2.76, 1.85, and 30.47, respectively]. Second, mitochondrial energy metabolism was activated, as evidenced by enrichment in oxidative phosphorylation and elevated levels of electron transport chain components [e.g., COX4 (cytochrome c oxidase subunit) and CYC2 (cytochrome c), with FC values of 1.63 and 1.53, respectively] and ATP synthase subunits [e.g., ATP4 (F-type ATP synthase subunit delta)]. Third, carbon and nitrogen assimilation capacity was strengthened, with up-regulation of carbon metabolism pathways (pentose phosphate pathway and pentose and glucuronate interconversions) and nitrogen metabolism pathways (arginine biosynthesis and alanine/aspartate/glutamate metabolism), accompanied by increased abundance of carbon metabolism enzymes [e.g., RPE1 (ribulose-phosphate 3-epimerase) and FBA1 (fructose-bisphosphate aldolase)] and the nitrogen assimilation enzyme GLN1 (glutamine synthetase; FC = 1.85, $p < 0.05$).

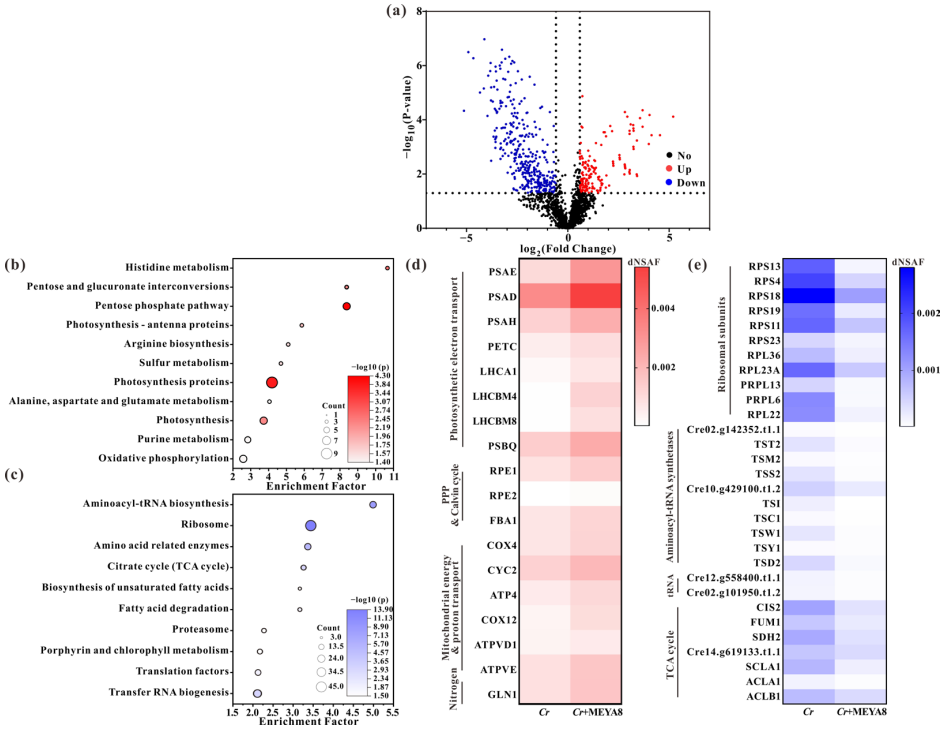

Figure 5. Proteomic pathway enrichment of differentially expressed proteins in *Chlamydomonas* under co-culture versus monoculture conditions. (**a**) Volcano plot of differentially expressed proteins in *Chlamydomonas* under co-culture versus monoculture conditions. The *x*-axis represents $\log_2$ fold change (co-culture/monoculture), and the *y*-axis represents $-\log_{10}$ (*p*-value). The horizontal dashed line indicates the significance threshold ($p < 0.05$), and the vertical dashed lines indicate the fold-change thresholds for upregulated and down-regulated proteins, corresponding to FC > 1.5 and FC < 0.66. Red dots: significantly upregulated proteins; blue: significantly down-regulated proteins; black dots: proteins with no significant difference. (**b**) KEGG pathway enrichment bubble plot of up-regulated proteins in *Chlamydomonas* under co-culture versus monoculture conditions. (**c**) KEGG pathway enrichment bubble plot of downregulated proteins in *Chlamydomonas* under co-culture versus mono-culture conditions. (**d**) Heatmap of key proteins in upregulated pathways under co-culture versus monoculture conditions. (**e**) Heatmap of key proteins in down-regulated pathways under co-culture versus monoculture conditions.

In contrast, the down-regulated proteins were dominated by proteins involved in genetic information processing and biosynthetic and metabolic activities (Figure 5c). The heatmap (Figure 5e) revealed comprehensive down-regulation of translational machinery, including multiple ribosomal proteins [e.g., RPS13 (40S ribosomal protein S13), RPS4 (40S ribosomal protein S4), RPL36 (60S ribosomal protein L36), and PRPL13 (ribosomal protein L13), with FC values of 0.07, 0.23, 0.26, and 0.18, respectively] and aminoacyl-tRNA synthetases [e.g., Cre02.g142352.t1.1 (histidyl-tRNA synthetase), TST2 (threonyl-tRNA synthetase), and TSM2 (methionyl-tRNA synthetase)]. Beyond translation, several proteins involved in other branches of central carbon metabolism, particularly TCA cycle-related enzymes such as CIS2 (citrate synthase; FC = 0.32), ACLA1 (ATP-citrate lyase A-1, Cre05.g241850.t1.2; FC = 0.29), and ATP-citrate synthase B-1, Cre02.g088600.t1.2; FC = 0.55)], lipid metabolism (fatty acid metabolism), and some proteins assigned to porphyrin and chlorophyll metabolism showed decreased abundance. Additionally, proteins associated with tRNA modification [e.g., Cre12.g558400.t1.1 (queuine tRNA-ribosyltransferase catalytic subunit 1)] showed reduced abundance.

4. Discussion

In this study, we isolated MEYA8, a previously uncharacterized bacterial strain that significantly stimulates the growth of the model microalga *Chlamydomonas reinhardtii*. Members of the genus *Cupriavidus* are extensively recognized for plant growth promotion [50,51], heavy metal resistance [52–54], xenobiotic degradation [55,56], and bioproduction [57,58]. However, its functional roles in microalgal growth promotion remain poorly characterized. Recent environmental surveys have occasionally detected *Cupriavidus* in specific aquatic niches, including the microbiomes of the marine dinoflagellate *Prorocentrum cordatum* [59], freshwater *Microcystis* blooms [60], and *Chlorella*–*Cupriavidus* consortia [61]. A preliminary screening of the global database "Microbial Community Database" (MiCoDa v2) [62] revealed that *Cupriavidus* has been detected in freshwater streams and lakes, wetlands, aquatic microbiomes, and other environmental samples, indicating its widespread presence in aquatic environments worldwide. Our findings demonstrate that *Cupriavidus* MEYA8 can be a new MGPB for *Chlamydomonas*, confirming its potential to establish beneficial interactions in the phycosphere and thereby expanding our understanding of algal–bacterial interactions. All these results suggest some *Cupriavidus* bacteria may play roles in the growth and function of phytoplankton, which have been largely overlooked in previous studies. However, more investigations are still needed in the future to better understand the ecological distributions and functional roles of *Cupriavidus* in the phycosphere.

Multi-omics data reveal that MEYA8 undergoes coordinated metabolic adaptations during co-culture. Phenotypic profiling showed that MEYA8 preferentially utilizes organic acids and amino acid derivatives (Figure 2c). These compounds are common components of algal exudates in the phycosphere [63], suggesting that MEYA8 may be adapted to use algal-derived metabolites during co-culture. Proteomic analysis confirmed this shift, with co-culture upregulation of pathways for central carbon/nitrogen metabolism, the pentose phosphate pathway, and glyoxylate/dicarboxylate metabolism, indicating enhanced substrate processing and energy generation. Specifically, the increased abundance of Acs and GckA suggest an enhanced capacity of MEYA8 to assimilate plausible algal-derived substrates, potentially involving acetate and photorespiration-associated C2/C3 metabolites such as glycolate and glycerate [64–68]. It should be noted that while these proteomic data indicate a strong potential for substrate assimilation, direct evidence of organic acid uptake will require future measurement of their extracellular concentrations during co-culture. Furthermore, members of the genus *Cupriavidus*, particularly *C. necator*, are well-established producers of polyhydroxyalkanoates (PHAs) under carbon-excess and nutrient-limited con-

ditions [69–71]. The observed upregulation of Acs and central carbon metabolic pathways in MEYA8 raises the possibility that assimilated algal-derived organic substrates could be channeled into acetyl-CoA and subsequently directed toward PHB/PHA biosynthesis. However, direct PHA quantification, analysis of the PhaA–PhaB–PhaC pathway, and stable-isotope tracing will be required to determine whether algal-derived carbon is incorporated into bacterial biopolymers, which would further highlight the biotechnological potential of this co-culture system.

In addition to carbon assimilation, co-cultivation also affected *Cupriavidus* pathways associated with aromatic amino acid and indole-related metabolism. Notably, key enzymes in tryptophan biosynthesis (TrpA/TrpB) were specifically upregulated (Figure 4d), supporting active IAA precursor production during interaction. MEYA8 harbors a complete IAA biosynthetic pathway and secretes IAA-like compounds based on Salkowski assay (Figure S2a,b). Furthermore, transwell assays demonstrate that MEYA8's stimulatory effect is mediated by a non-contact, diffusible factor. Our exogenous IAA assays showed that low concentrations (0.5 mg L^{-1}) promoted *Chlamydomonas* proliferation, while higher levels were inhibitory (Figure S2c,d), consistent with typical hormetic responses [12,72]. These dose-dependent results are also consistent with the effects of bacterial cell density on *Chlamydomonas* growth, where only an optimum ratio yields a strong growth stimulation (Figure 1a). These results collectively re-highlight that IAA or other indole-related metabolites can greatly contribute to the mutualistic algal–bacterial interactions.

Other metabolites may also contribute to this growth-promoting effect. Despite overall population growth, MEYA8 downregulated ribosomal and DNA replication proteins during co-culture, suggesting a physiological transition from rapid proliferation to a resource-efficient, phycosphere-adapted state optimized for metabolic exchange. This metabolic remodeling likely provides the energetic and biosynthetic basis for sustained production of diffusible growth-promoting factors. Although IAA is a strong candidate mediator, the growth-promoting effect of MEYA8 is unlikely to be explained by a single metabolite. Exogenous VB_1 and VB_7 showed no clear growth-promoting effect here (Figure S2e–h), despite their known role in other systems [22,73]. However, the coordinated upregulation of aromatic amino acid biosynthesis proteins (such as AroQ, AroC, TyrB) (Figure 4d) suggests enhanced production of indole-related metabolites beyond IAA. The increased utilization of microalgal-derived organic acids and amino acid derivatives may provide the metabolic resources required for sustained synthesis of growth-promoting compounds. Previous studies have shown that bacteria associated with microalgae can influence host physiology through multiple mechanisms, including siderophore production, volatile organic compounds, and extracellular polymeric substances [26,74]. Therefore, the stimulatory effect of MEYA8 may result from the combined action of IAA-like compounds and additional metabolites that remain to be identified. Further genetic and metabolomic analyses will be required to resolve the relative contribution of these factors.

The *Chlamydomonas* proteomic data revealed that co-cultivation has greatly altered the abundance of various metabolic and regulatory proteins in the microalga. Co-culture upregulated proteins involved in photosynthetic electron transport, light harvesting, and mitochondrial ATP generation (Figure 5d), directly corroborating physiological improvements in Fv/Fm and chlorophyll accumulation (Figure 1a,d). Concurrently, carbon metabolism and nitrogen assimilation proteins were enriched. These upregulated processes suggest enhanced photosynthetic energy capture and altered nutrient assimilation during co-cultivation. In contrast, translational machinery, aminoacyl-tRNA biosynthesis, and biosynthetic pathways (TCA cycle, fatty acid metabolism) (Figure 5e) were downregulated, representing reduced abundance of translational machinery and altered biosynthetic activity. Although this pattern may be consistent with changes in cellular resource alloca-

tion, it should not be interpreted solely as an adaptive strategy. Reduced abundance of translational machinery may also reflect differences in specific growth rate, growth phase, cell-division activity, cellular composition, metabolic acclimation, or physiological stress at the time of sampling [75–78]. Taken together, the current findings provide a model of reciprocal metabolic interaction in which bacterial metabolites influence algal physiology and algal-derived substrates potentially sustain bacterial metabolic activity. This supports the view that the phycosphere functions not merely as a nutrient-sharing microenvironment but as a metabolically interactive niche in which bacterial metabolites influence algal physiology and algal exudates support bacterial metabolic specialization [79,80].

Our results may provide new insights into the use of MGPBs to enhance microalgal productivity [81]. Tailored bacterial partners could replace costly additives, improving productivity and culture stability [82], while well-characterized strains like MEYA8 may enhance system resilience in open photobioreactors by modulating phycosphere dynamics [83]. However, some key limitations still need to be addressed: the long-term consortium stability needs validation in pilot-scale systems. Moreover, the targeted LC-MS/MS analysis using authentic standards, combined with gene knockout and complementation of candidate indole-metabolite biosynthetic pathways, should be required to identify and quantify the active compounds. Future work should prioritize genetic dissection of bacterial metabolite pathways and the rational design of synthetic consortia to transition algal–bacterial mutualisms from laboratory models to scalable bioproduction platforms.

5. Conclusions

In this study, we isolated *Cupriavidus* MEYA8 as a growth-promoting bacterium for *Chlamydomonas reinhardtii*. The growth-promoting effect varied with the bacterial inoculation ratio, while transwell assays suggested that diffusible factors contribute to the interaction. Genomic and proteomic analyses revealed that MEYA8 is well adapted to the *Chlamydomonas* phycosphere, preferentially utilizing microalgal-derived organic acids and amino acid derivatives. *Chlamydomonas* upregulated photosynthetic, energy metabolism, and nutrient assimilation proteins while downregulating translational and biosynthetic machinery. This study provides new insight into algal–bacterial interactions and highlights MEYA8 as a promising bacterial partner for improving algal cultivation.

Supplementary Materials: The following supporting information can be downloaded at: https://www.mdpi.com/article/10.3390/phycology6030089/s1, Figure S1: (a) Chlorophyll content of *Chlamydomonas* (Cr) after 7 days of co-culture with different bacteria (25 °C, continuous light at 120 μmol photons m^{-2} s^{-1}). (b) Growth-promoting phenotype of strain MEYA8 on *Chlamydomonas* at an initial inoculum ratio of 100:1 (Bacterial cell: Algal cell). Data are presented as mean ± SD (n = 3). Statistical significance was determined by t-test. Asterisks indicate significant differences from the axenic control (** $p < 0.01$, *** $p < 0.001$); Figure S2: IAA biosynthetic pathway, secretion ability, and dose-dependent growth-promoting effects of exogenous IAA and vitamin on *Chlamydomonas*. (a) IAA biosynthetic pathway. PRA: N-(5-Phospho-D-ribosyl) anthranilate, CdRP: 1-(2-Carboxyphenylamino)-1-deoxy-D-ribulose 5-phosphate, IGP: indole-3-glycerol phosphate, Trp: tryptophan, IPyA: indole-3-pyruvate, IAAld: indole-3-acetaldehyde, IAA: indole-3-acetate. (b) Characterization of IAA secretion ability of strain MEYA8. NC: Negative control (non-inoculated medium); T: Strain MEYA8 culture. (c,d) Dose-dependent growth-promoting effects of exogenous IAA on *Chlamydomonas*. Cell density (c) and total chlorophyll content (d) were determined at day 10. Dose-dependent responses of *Chlamydomonas* to exogenous vitamin on Day 10. (e,f) VB_1; (g,h) VB_7. [Values are means ± SD (n = 3). Statistical significance was determined by t-test. Asterisks indicate significant differences from the control: * $p < 0.05$, ** $p < 0.01$, *** $p < 0.001$, and **** $p < 0.0001$]; Table S1: Genes for IAA, thiamine, and biotin biosynthesis in starin MEYA8; Table S2: Differentially expressed proteins of *Cupriavidus*

MEYA8 when comparing co-cultures vs monocultures. Table S3: Differentially expressed proteins of *Chlamydomonas* when comparing co-cultures vs monocultures.

Author Contributions: Conceptualization, B.X.; methodology, X.W., X.L., M.S., J.Y., Y.W. and B.X.; validation, X.L., M.S., J.Y. and B.X.; formal analysis, X.W. and X.L.; investigation, X.W., X.L., M.S., J.Y., Y.W. and B.X.; resources, X.L. and B.X.; data curation, X.W., X.L., Y.W. and B.X.; writing—original draft, X.W.; writing—review & editing, X.W., Y.W. and B.X.; visualization, X.W. and Y.J.; project administration, Y.W. and B.X.; funding acquisition, Y.W. and B.X.; software, Y.J.; supervision, Y.W. and B.X. All authors have read and agreed to the published version of the manuscript.

Funding: This research was funded by the National Key Research and Development Program of China (2023YFC3207804 to B.X), the National Natural Science Foundation of China (31970109 and 31570098 to B.X; 32100094 to Y.W.), Hubei International Scientific and Technological Cooperation Base of Ecology and Environment (GH202502 to Y.W.), and Fundamental Research Funds for the Central Universities (30106260152 to Y.W.).

Institutional Review Board Statement: Not applicable.

Informed Consent Statement: Not applicable.

Data Availability Statement: The genome sequence data generated in this study have been deposited in the National Center for Biotechnology Information (NCBI) database under accession number PRJNA1482777. Mass spectrometry proteomics data have been deposited in the ProteomeXchange Consortium database (http://proteomecentral.proteomexchange.org) via the iProX partner repository [84,85] with the data set identifier IPX0017963000.

Conflicts of Interest: The authors declare no conflicts of interest.

References

1. Cheah, W.Y.; Ling, T.C.; Show, P.L.; Juan, J.C.; Chang, J.-S.; Lee, D.-J. Cultivation in wastewaters for energy: A microalgae platform. *Appl. Energy* **2016**, *179*, 609–625. [CrossRef]
2. Schroda, M.; Remacle, C. Molecular advancements establishing *Chlamydomonas* as a host for biotechnological exploitation. *Front. Plant Sci.* **2022**, *13*, 911483. [CrossRef]
3. da Silva Pessoa, J.; de Oliveira, C.F.M.; Mena-Chalco, J.P.; de Carvalho, J.C.M.; Ferreira-Camargo, L.S. Trends on *Chlamydomonas reinhardtii* growth regimes and bioproducts. *Biotechnol. Appl. Biochem.* **2023**, *70*, 1830–1842. [CrossRef]
4. Wayne, B.; Ralph, M. Chemotactic and growth responses of marine bacteria to algal extracellular products. *Biol. Bull.* **1972**, *143*, 265–277. [CrossRef] [PubMed]
5. Cole, J.J. Interactions between bacteria and algae in aquatic ecosystems. *Annu. Rev. Ecol. Syst.* **1982**, *13*, 291–314. [CrossRef]
6. Kimbrel, J.A.; Samo, T.J.; Ward, C.; Nilson, D.; Thelen, M.P.; Siccardi, A.; Zimba, P.; Lane, T.W.; Mayali, X. Host selection and stochastic effects influence bacterial community assembly on the microalgal phycosphere. *Algal Res.* **2019**, *40*, 101489. [CrossRef]
7. Jackrel, S.L.; Yang, J.W.; Schmidt, K.C.; Denef, V.J. Host specificity of microbiome assembly and its fitness effects in phytoplankton. *ISME J.* **2021**, *15*, 774–788. [PubMed]
8. Bai, Y.; Mori, K.; Tanaka, Y.; Toyama, T. Isolation and characterization of bacteria from natural microbiota regrown with *Chlamydomonas reinhardtii* in synthetic co-cultures. *Algal Res.* **2025**, *86*, 103954. [CrossRef]
9. Toyama, T.; Kasuya, M.; Hanaoka, T.; Kobayashi, N.; Tanaka, Y.; Inoue, D.; Sei, K.; Morikawa, M.; Mori, K. Growth promotion of three microalgae, *Chlamydomonas reinhardtii*, *Chlorella vulgaris* and *Euglena gracilis*, by in situ indigenous bacteria in wastewater effluent. *Biotechnol. Biofuels* **2018**, *11*, 176. [CrossRef] [PubMed]
10. Durán, P.; Flores-Uribe, J.; Wippel, K.; Zhang, P.; Guan, R.; Melkonian, B.; Melkonian, M.; Garrido-Oter, R. Shared features and reciprocal complementation of the *Chlamydomonas* and *Arabidopsis* microbiota. *Nat. Commun.* **2022**, *13*, 406. [CrossRef] [PubMed]
11. Palacios, O.A.; López, B.R.; de-Bashan, L.E. Microalga Growth-Promoting Bacteria (MGPB): A formal term proposed for beneficial bacteria involved in microalgal–bacterial interactions. *Algal Res.* **2022**, *61*, 102585. [CrossRef]
12. Cheng, X.; Li, X.; Tong, M.; Wu, J.; Chan, L.L.; Cai, Z.; Zhou, J. Indole-3-acetic acid as a cross-talking molecule in algal–bacterial interactions and a potential driving force in algal bloom formation. *Front. Microbiol.* **2023**, *14*, 1236925. [CrossRef] [PubMed]
13. Wu, X.; Kong, L.; Feng, Y.; Zheng, R.; Zhou, J.; Sun, J.; Liu, S. Communication mediated interaction between bacteria and microalgae advances photogranulation. *Sci. Total Environ.* **2024**, *914*, 169975. [CrossRef] [PubMed]
14. Dao, G.; Wu, G.; Wang, X.; Zhang, T.; Zhan, X.; Hu, H. Enhanced microalgae growth through stimulated secretion of indole acetic acid by symbiotic bacteria. *Algal Res.* **2018**, *33*, 345–351. [CrossRef]

15. Palacios, O.A.; Gomez-Anduro, G.; Bashan, Y.; de-Bashan, L.E. Tryptophan, thiamine and indole-3-acetic acid exchange between *Chlorella sorokiniana* and the plant growth-promoting bacterium *Azospirillum brasilense*. *FEMS Microbiol. Ecol.* **2016**, *92*, fiw077. [CrossRef] [PubMed]
16. Hernandez, J.-P.; de-Bashan, L.E.; Rodriguez, D.J.; Rodriguez, Y.; Bashan, Y. Growth promotion of the freshwater microalga *Chlorella vulgaris* by the nitrogen-fixing, plant growth-promoting bacterium *Bacillus pumilus* from arid zone soils. *Eur. J. Soil. Biol.* **2009**, *45*, 88–93. [CrossRef]
17. Villa, J.A.; Ray, E.E.; Barney, B.M. *Azotobacter vinelandii* siderophore can provide nitrogen to support the culture of the green algae *Neochloris oleoabundans* and *Scenedesmus* sp. BA032. *FEMS Microbiol. Lett.* **2014**, *351*, 70–77. [CrossRef] [PubMed]
18. Aburai, N.; Tsukagoshi, T.; Sekiguchi, S.; Arakawa, H.; Imamura, Y.; Abe, K. Mutual supply of carbon and nitrogen sources in the co-culture of aerial microalgae and nitrogen-fixing bacteria. *Algal Res.* **2023**, *70*, 103001. [CrossRef]
19. Keshtacher-Liebso, E.; Hadar, Y.; Chen, Y. Oligotrophic bacteria enhance algal growth under iron deficient conditions. *Appl. Environ. Microbiol.* **1995**, *61*, 2439–2441. [CrossRef] [PubMed]
20. Rawat, D.; Sharma, U.; Poria, P.; Finlan, A.; Parker, B.; Sharma, R.S.; Mishra, V. Iron-dependent mutualism between *Chlorella sorokiniana* and *Ralstonia pickettii* forms the basis for a sustainable bioremediation system. *ISME Commun.* **2022**, *2*, 83. [CrossRef] [PubMed]
21. Rajapitamahuni, S.; Bhayani, K.; Bachani, P.; Bharadwaj, S.V.V.; Mishra, S. An effective approach of bacterial siderophore as nitrogen source triggering the desired biochemical changes in microalgae *Chlorella variabilis* ATCC 12198. *Algal Res.* **2019**, *43*, 101610. [CrossRef]
22. Amin, S.A.; Green, D.H.; Hart, M.C.; Küpper, F.C.; Sunda, W.G.; Carrano, C.J. Photolysis of iron-siderophore chelates promotes bacterial-algal mutualism. *Proc. Natl. Acad. Sci. USA* **2009**, *106*, 17071–17076. [CrossRef] [PubMed]
23. Croft, M.T.; Lawrence, A.D.; Raux-Deery, E.; Warren, M.J.; Smith, A.G. Algae acquire vitamin B_{12} through a symbiotic relationship with bacteria. *Nature* **2005**, *438*, 90–93. [CrossRef] [PubMed]
24. Croft, M.T.; Warren, M.J.; Smith, A.G. Algae need their vitamins. *Eukaryot. Cell* **2006**, *5*, 1175–1183. [CrossRef] [PubMed]
25. Kazamia, E.; Czesnick, H.; Nguyen, T.T.V.; Croft, M.T.; Sherwood, E.; Sasso, S.; Hodson, S.J.; Warren, M.J.; Smith, A.G. Mutualistic interactions between vitamin B_{12}-dependent algae and heterotrophic bacteria exhibit regulation. *Environ. Microbiol.* **2012**, *14*, 1466–1476. [CrossRef] [PubMed]
26. Fuentes, J.L.; Garbayo, I.; Cuaresma, M.; Montero, Z.; González-Del-Valle, M.; Vílchez, C. Impact of microalgae-bacteria interactions on the production of algal biomass and associated compounds. *Mar. Drugs* **2016**, *14*, 100. [CrossRef] [PubMed]
27. You, X.; Chen, Q.; Kong, L.; Feng, Y.; Hu, J.; Liu, S.; Sun, W. Antibiotic stress–induced hormesis in phytoplankton and bacteria through their mutual cooperation. *Sci. Adv.* **2025**, *11*, eadv7921. [CrossRef] [PubMed]
28. Toyama, T.; Hanaoka, T.; Yamada, K.; Suzuki, K.; Tanaka, Y.; Morikawa, M.; Mori, K. Enhanced production of biomass and lipids by *Euglena gracilis* via co-culturing with a microalga growth-promoting bacterium, *Emticicia* sp. EG3. *Biotechnol. Biofuels* **2019**, *12*, 205. [CrossRef] [PubMed]
29. Jeon, M.S.; Han, S.-I.; Ahn, J.-W.; Jung, J.-H.; Choi, J.-S.; Choi, Y.-E. Endophyte *Bacillus tequilensis* improves the growth of microalgae *Haematococcus lacustris* by regulating host cell metabolism. *Bioresour. Technol.* **2023**, *387*, 129546. [CrossRef] [PubMed]
30. Sauvage, J.; Wikfors, G.H.; Dixon, M.S.; Kapareiko, D.; Sabbe, K.; Li, X.; Joyce, A. Bacterial exudates as growth-promoting agents for the cultivation of commercially relevant marine microalgal strains. *J. World Aquacult. Soc.* **2022**, *53*, 1101–1119. [CrossRef]
31. Li, Q.; Li, Y.; Pei, H. Algal–bacterial consortia for bioproduct generation and wastewater treatment. *Renew. Sustain. Energy Rev.* **2021**, *149*, 111395. [CrossRef]
32. Gorman, D.S.; Levine, R.P. Cytochrome f and plastocyanin: Their sequence in the photosynthetic electron transport chain of *Chlamydomonas reinhardtii*. *Proc. Natl. Acad. Sci. USA* **1965**, *54*, 1665–1669. [CrossRef] [PubMed]
33. Beringer, J.E. R Factor Transfer in *Rhizobium leguminosarum*. *Microbiology* **1974**, *84*, 188–198. [CrossRef] [PubMed]
34. Lane, D.J.; Pace, B.; Olsen, G.J.; Stahl, D.A.; Sogin, M.L.; Pace, N.R. Rapid determination of 16S ribosomal RNA sequences for phylogenetic analyses. *Proc. Natl. Acad. Sci. USA* **1985**, *82*, 6955–6959. [CrossRef] [PubMed]
35. Yoon, S.H.; Ha, S.M.; Kwon, S.; Lim, J.; Kim, Y.; Seo, H.; Chun, J. Introducing EzBioCloud: A taxonomically united database of 16S rRNA and whole genome assemblies. *Int. J. Syst. Evol. Microbiol.* **2017**, *67*, 1613–1617. [CrossRef] [PubMed]
36. Freese, H.M.; Meier-Kolthoff, J.P.; Göker, M. TYGS and LPSN in 2025: A Global Core Biodata Resource for genome-based classification and nomenclature of prokaryotes within DSMZ Digital Diversity. *Nucleic Acids Res.* **2025**, *54*, D884–D891. [CrossRef] [PubMed]
37. Gordon, S.A.; Weber, R.P. Colorimetric estimation of indoleacetic acid. *Plant Physiol.* **1951**, *26*, 192–195. [CrossRef] [PubMed]
38. Glickmann, E.; Dessaux, Y. A critical examination of the specificity of the salkowski reagent for indolic compounds produced by phyto-pathogenic bacteria. *Appl. Environ. Microbiol.* **1995**, *61*, 793–796. [CrossRef] [PubMed]
39. Sueoka, N. Mitotic replication of deoxyribonucleic acid in *Chlamydomonas reinhardtii*. *Proc. Natl. Acad. Sci. USA* **1960**, *46*, 83–91. [CrossRef] [PubMed]

40. Minocha, R.; Martinez, G.; Lyons, B.; Long, S. Development of a standardized methodology for quantifying total chlorophyll and carotenoids from foliage of hardwood and conifer tree species. *Can. J. For. Res.* **2009**, *39*, 849–861. [CrossRef]
41. Zhao, N.; Wang, B.; Liu, F.; Xie, B. Sample preparation of microorganism for label-free quantitative proteomics. *Bio-101* **2021**, e2003595. [CrossRef]
42. Zhao, N.; Liu, F.; Dong, W.; Halverson, L.J.; Xie, B. Quantitative proteomics insights into *Chlamydomonas reinhardtii* thermal tolerance enhancement by a mutualistic interaction with *Sinorhizobium meliloti*. *Microbiol. Spectr.* **2024**, *12*, e0021924. [CrossRef] [PubMed]
43. Christie-Oleza, J.A.; Sousoni, D.; Lloyd, M.; Armengaud, J.; Scanlan, D.J. Nutrient recycling facilitates long-term stability of marine microbial phototroph–heterotroph interactions. *Nat. Microbiol.* **2017**, *2*, 17100. [CrossRef] [PubMed]
44. Zhang, Y.; Wen, Z.; Washburn, M.P.; Florens, L. Refinements to label free proteome quantitation: How to deal with peptides shared by multiple proteins. *Anal. Chem.* **2010**, *82*, 2272–2281. [CrossRef] [PubMed]
45. Chen, C.; Wu, Y.; Li, J.; Wang, X.; Zeng, Z.; Xu, J.; Liu, Y.; Feng, J.; Chen, H.; He, Y.; et al. TBtools-II: A "one for all, all for one" bioinformatics platform for biological big-data mining. *Mol. Plant.* **2023**, *16*, 1733–1742. [CrossRef] [PubMed]
46. Chun, J.; Oren, A.; Ventosa, A.; Christensen, H.; Arahal, D.R.; da Costa, M.S.; Rooney, A.P.; Yi, H.; Xu, X.W.; De Meyer, S.; et al. Proposed minimal standards for the use of genome data for the taxonomy of prokaryotes. *Int. J. Syst. Evol. Microbiol.* **2018**, *68*, 461–466. [CrossRef] [PubMed]
47. Lykidis, A.; Pérez-Pantoja, D.; Ledger, T.; Mavromatis, K.; Anderson, I.J.; Ivanova, N.N.; Hooper, S.D.; Lapidus, A.; Lucas, S.; González, B.; et al. The complete multipartite genome sequence of *Cupriavidus necator* JMP134, a versatile pollutant degrader. *PLoS ONE* **2010**, *5*, e9729. [CrossRef] [PubMed]
48. Janssen, P.J.; Van Houdt, R.; Moors, H.; Monsieurs, P.; Morin, N.; Michaux, A.; Benotmane, M.A.; Leys, N.; Vallaeys, T.; Lapidus, A.; et al. The complete genome sequence of *Cupriavidus metallidurans* strain CH34, a master Survivalist in harsh and anthropogenic environments. *PLoS ONE* **2010**, *5*, e10433. [CrossRef] [PubMed]
49. Yang, Z.; Zhang, S.; Li, X. Complete genome sequence of *Cupriavidus* sp. Agwp_2, isolated from soil in an iron mining area. *Microbiol. Resour. Announc* **2025**, *14*, e0088424. [CrossRef] [PubMed]
50. Ramandi, A.; Jaghargh, M.B.; Nourashrafeddin, S.M.; Seifi, A. *Cupriavidus metallidurans*: A species-non-specific and multifaceted plant growth-promoting bacteria. *BMC Plant Biol.* **2024**, *24*, 1197. [CrossRef] [PubMed]
51. Zúñiga, A.; Fuente, F.D.L.; Federici, F.; Lionne, C.; Bônnet, J.; Lorenzo, V.D.; González, B. An engineered device for indoleacetic acid production under quorum sensing signals enables *Cupriavidus pinatubonensis* JMP134 to stimulate plant growth. *ACS Synth. Biol.* **2018**, *7*, 1519–1527. [CrossRef] [PubMed]
52. Vicentin, R.P.; Santos, J.V.D.; Labory, C.R.G.; Costa, A.M.D.; Moreira, F.M.D.S.; Alvesi, E. Tolerance to and accumulation of Cadmium, Copper, and Zinc by *Cupriavidus necator*. *Rev. Bras. Ciência Solo* **2018**, *42*, e0170080. [CrossRef]
53. Klonowska, A.; Moulin, L.; Ardley, J.K.; Braun, F.; Gollagher, M.M.; Zandberg, J.D.; Marinova, D.V.; Huntemann, M.; Reddy, T.B.K.; Varghese, N.J.; et al. Novel heavy metal resistance gene clusters are present in the genome of *Cupriavidus neocaledonicus* STM 6070, a new species of *Mimosa pudica* microsymbiont isolated from heavy-metal-rich mining site soil. *BMC Genom.* **2020**, *21*, 214. [CrossRef] [PubMed]
54. Hirth, N.; Gerlach, M.S.; Wiesemann, N.; Herzberg, M.; Große, C.; Nies, D.H. Full copper resistance in *Cupriavidus metallidurans* requires the interplay of many resistance systems. *Appl. Environ. Microbiol.* **2023**, *89*, e0056723. [CrossRef] [PubMed]
55. Pérez-Pantoja, D.; Iglesia, R.D.L.; Pieper, D.H.; González, B. Metabolic reconstruction of aromatic compounds degradation from the genome of the amazing pollutant-degrading bacterium *Cupriavidus necator* JMP134. *FEMS Microbiol. Rev.* **2008**, *32*, 736–794. [CrossRef] [PubMed]
56. Sathesh-Prabu, C.; Woo, J.; Kim, Y.; Kim, S.M.; Lee, S.B.; Jeon, C.O.; Kim, D.; Lee, S.K. Comparative genomic analysis and BTEX degradation pathways of a thermotolerant *Cupriavidus cauae* PHS1. *J. Microbiol. Biotechnol.* **2023**, *33*, 875–885. [CrossRef] [PubMed]
57. Sohn, Y.J.; Son, J.; Jo, S.Y.; Park, S.Y.; Yoo, J.I.; Baritugo, K.-A.; Na, J.G.; Choi, J.-I.; Kim, H.T.; Joo, J.C.; et al. Chemoautotroph *Cupriavidus necator* as a potential game-changer for global warming and plastic waste problem: A review. *Bioresour. Technol.* **2021**, *340*, 125693. [CrossRef] [PubMed]
58. Obruca, S.; Marova, I.; Snajdar, O.; Mravcova, L.; Svoboda, Z. Production of poly(3-hydroxybutyrate-co-3-hydroxyvalerate) by *Cupriavidus necator* from waste rapeseed oil using propanol as a precursor of 3-hydroxyvalerate. *Biotechnol. Lett.* **2010**, *32*, 1925–1932. [CrossRef] [PubMed]
59. Sanchez-Garcia, S.; Wang, H.; Wagner-Döbler, I. The microbiome of the dinoflagellate *Prorocentrum cordatum* in laboratory culture and its changes at higher temperatures. *Front. Microbiol.* **2022**, *13*, 952238. [CrossRef] [PubMed]
60. Samuel, P.S.; Lopez, J.V. Diversity fluctuations of the microbial community during annual *Microcystis* blooms within Lake Okeechobee, FL. *Front. Water* **2025**, *7*, 1678547. [CrossRef]
61. Yi, T.; Shan, Y.; Huang, B.; Tang, T.; Wei, W.; Quinn, N.W.T. An efficient *Chlorella* sp.-*Cupriavidus necator* microcosm for phenol degradation and its cooperation mechanism. *Sci. Total Environ.* **2020**, *743*, 140775. [CrossRef] [PubMed]
62. Jurburg, S.; Arboleda-Baena, C.; Kazem, A.; Frøslev, T.; Jeppesen, T. *Microbial Community Database (MiCoDa)*; v2 [Database]; German Centre for Integrative Biodiversity Research (iDiv) Halle–Jena–Leipzig: Leipzig, Germany, 2024.

63. Seymour, J.R.; Amin, S.A.; Raina, J.-B.; Stocker, R. Zooming in on the phycosphere: The ecological interface for phytoplankton–bacteria relationships. *Nat. Microbiol.* **2017**, *2*, 17065. [CrossRef] [PubMed]
64. Kumari, S.; Tishel, R.; Eisenbach, M.; Wolfe, A.J. Cloning, characterization, and functional expression of *acs*, the gene which encodes acetyl coenzyme A synthetase in *Escherichia coli*. *J. Bacteriol.* **1995**, *177*, 2878–2886. [CrossRef] [PubMed]
65. Chistoserdova, L.; Lidstrom, M.E. Identification and mutation of a gene required for glycerate kinase activity from a facultative methylotroph, *Methylobacterium extorquens* AM1. *J. Bacteriol.* **1997**, *179*, 4946–4948. [CrossRef] [PubMed]
66. Kaplan, A.; Berry, J.A. Glycolate excretion and the oxygen to carbon dioxide net exchange ratio during photosynthesis in *Chlamydomonas reinhardtii*. *Plant Physiol.* **1981**, *67*, 229–232. [CrossRef] [PubMed]
67. Moroney, J.V.; Wilson, B.J.; Tolbert, N.E. Glycolate metabolism and excretion by *Chlamydomonas reinhardtii*. *Plant Physiol.* **1986**, *82*, 821–826. [CrossRef] [PubMed]
68. Yang, W.; Catalanotti, C.; D'Adamo, S.; Wittkopp, T.M.; Ingram-Smith, C.J.; Mackinder, L.; Miller, T.E.; Heuberger, A.L.; Peers, G.; Smith, K.S.; et al. Alternative acetate production pathways in *Chlamydomonas reinhardtii* during dark anoxia and the dominant role of chloroplasts in fermentative acetate production. *Plant Cell* **2014**, *26*, 4499–4518. [CrossRef] [PubMed]
69. Reinecke, F.; Steinbüchel, A. *Ralstonia eutropha* strain H16 as model organism for PHA metabolism and for biotechnological production of technically interesting biopolymers. *J. Mol. Microbiol. Biotechnol.* **2009**, *16*, 91–108. [CrossRef] [PubMed]
70. Marudkla, J.; Lee, W.-C.; Wannawilai, S.; Chisti, Y.; Sirisansaneeyakul, S. Model of acetic acid-affected growth and poly(3-hydroxybutyrate) production by *Cupriavidus necator* DSM 545. *J. Biotechnol.* **2018**, *268*, 12–20. [CrossRef] [PubMed]
71. Cai, F.; Lin, M.; Jin, W.; Chen, C.; Liu, G. Biosynthesis of poly(3-hydroxybutyrate-co-3-hydroxyvalerate) from volatile fatty acids by *Cupriavidus necator*. *J. Basic Microbiol.* **2023**, *63*, 128–139. [CrossRef] [PubMed]
72. Chung, T.Y.; Kuo, C.Y.; Lin, W.J.; Wang, W.L.; Chou, J.Y. Indole-3-acetic-acid-induced phenotypic plasticity in *Desmodesmus* algae. *Sci. Rep.* **2018**, *8*, 10270. [CrossRef] [PubMed]
73. Yao, S.; Lyu, S.; An, Y.; Lu, J.; Gjermansen, C.; Schramm, A. Microalgae–bacteria symbiosis in microalgal growth and biofuel production: A review. *J. Appl. Microbiol.* **2019**, *126*, 359–368. [CrossRef] [PubMed]
74. Oruganti, R.K.; Vahedi, S.; Das, D. A comprehensive review on the use of algal-bacterial systems for wastewater treatment and resource recovery. *Bioresour. Technol.* **2022**, *344*, 126230.
75. Schmollinger, S.; Mühlhaus, T.; Boyle, N.R.; Blaby, I.K.; Casero, D.; Mettler, T.; Moseley, J.L.; Kropat, J.; Sommer, F.; Strenkert, D.; et al. Nitrogen-sparing mechanisms in *Chlamydomonas* affect the transcriptome, the proteome, and photosynthetic metabolism. *Plant Cell* **2014**, *26*, 1410–1435. [CrossRef] [PubMed]
76. Park, J.-J.; Wang, H.; Gargouri, M.; Deshpande, R.R.; Skepper, J.N.; Holguin, F.O.; Juergens, M.T.; Shachar-Hill, Y.; Hicks, L.M.; Gang, D.R. The response of *Chlamydomonas reinhardtii* to nitrogen deprivation: A systems biology analysis. *Plant J.* **2015**, *81*, 611–624. [CrossRef] [PubMed]
77. Zones, J.M.; Blaby, I.K.; Merchant, S.S.; Umen, J.G. High-resolution profiling of a synchronized diurnal transcriptome from *Chlamydomonas reinhardtii* reveals continuous cell and metabolic differentiation. *Plant Cell* **2015**, *27*, 2743–2769. [CrossRef] [PubMed]
78. Miller, R.; Wu, G.; Deshpande, R.R.; Vieler, A.; Gärtner, K.; Li, X.; Moellering, E.R.; Zäuner, S.; Cornish, A.J.; Liu, B.; et al. Changes in transcript abundance in *Chlamydomonas reinhardtii* following nitrogen deprivation predict diversion of metabolism. *Plant Physiol.* **2010**, *154*, 1737–1752. [CrossRef] [PubMed]
79. Burgunter-Delamare, B.; Shetty, P.; Vuong, T.; Mittag, M. Exchange or eliminate: The secrets of algal–bacterial relationships. *Plants* **2024**, *13*, 829. [CrossRef] [PubMed]
80. González-González, L.M.; de-Bashan, L.E.; Bashan, Y. Toward the enhancement of microalgal metabolite production through microalgae–bacteria consortia. *Biology* **2021**, *10*, 282. [CrossRef] [PubMed]
81. Kim, B.-H.; Ramanan, R.; Cho, D.-H.; Oh, H.-M.; Kim, H.-S. Role of *Rhizobium*, a plant growth promoting bacterium, in enhancing algal biomass through mutualistic interaction. *Biomass Bioenergy* **2014**, *69*, 95–105. [CrossRef]
82. Pathom-Aree, W.; Sattayawat, P.; Inwongwan, S.; Cheirsilp, B.; Liewtrakula, N.; Maneechote, W.; Rangseekaew, P.; Ahmad, F.; Mehmood, M.A.; Gao, F.; et al. Microalgae growth-promoting bacteria for cultivation strategies: Recent updates and progress. *Microbiol. Res.* **2024**, *286*, 127813. [CrossRef] [PubMed]
83. Chevanton, M.L.; Garnier, M.; Bougaran, G.; Schreiber, N.; Lukomska, E.; Bérard, J.-B.; Fouilland, E.; Bernard, O.; Cadoret, J.-P. Screening and selection of growth-promoting bacteria for *Dunaliella* cultures. *Algal Res.* **2013**, *2*, 212–222. [CrossRef]
84. Ma, J.; Chen, T.; Wu, S.; Yang, C.; Bai, M.; Shu, K.; Li, K.; Zhang, G.; Jin, Z.; He, F.; et al. iProX: An integrated proteome resource. *Nucleic Acids Res.* **2019**, *47*, D1211–D1217. [CrossRef] [PubMed]
85. Chen, T.; Ma, J.; Liu, Y.; Chen, Z.; Xiao, N.; Lu, Y.; Fu, Y.; Yang, C.; Li, M.; Wu, S.; et al. iProX in 2021: Connecting proteomics data sharing with big data. *Nucleic Acids Res.* **2022**, *50*, D1522–D1527. [CrossRef] [PubMed]

Disclaimer/Publisher's Note: The statements, opinions and data contained in all publications are solely those of the individual author(s) and contributor(s) and not of MDPI and/or the editor(s). MDPI and/or the editor(s) disclaim responsibility for any injury to people or property resulting from any ideas, methods, instructions or products referred to in the content.